Asian Journal of Chemistry; Vol. 37, No. 10 (2025), 2589-2598
ASIAN JOURNAL OF CHEMISTRY
https://doi.org/10.14233/ajchem.2025.34511

Tailoring NiO Thin Films: Citric Acid-Assisted Synthesis and Cobalt Doping for Enhanced Properties

V. RADHA JAYALAKSHMI[1] and N. JEYAKUMARAN[2,*]

[1]Department of Physics, E.M.G. Yadava Women's College, Madurai-625014, India
[2]Department of Physics, V.H.N. Senthikumara Nadar College, Virudhunagar-626001, India

*Corresponding author: E-mail: jeyakumaran@vhnsnc.edu.in

Received: 22 July 2025 *Accepted*: 25 September 2025 *Published online*: 30 September 2025 AJC-22144

This study investigates the cobalt doped nickel oxide ssthin films synthesis using a sol-gel method using citric acid as chelating agent combined with spin-coating techniques. The structural, chemical and morphological characteristics of pure NiO, 1%, 3%, 5% and 7% Co doped NiO thin films were examined. Also, effects of annealing temperatures (400 ºC, 500 ºC and 600 ºC) were studied on pure NiO and Co doped NiO. X-ray diffraction (XRD) confirmed a polycrystalline cubic structure with increased crystallinity and the reduced defect states were observed at higher annealing temperatures, particularly at 600 ºC. The UV Visible spectroscopy results revealed the significant transmittance in annealed NiO thin films, with the band gap energy decreasing from 3.72 eV to 2.89 eV as the annealing temperature increased. The X-ray photoelectron spectroscopy (XPS), O 1s spectra revealed the presence of lattice oxygen, surface hydroxyl groups and Ni_2O_3, with a significant reduction in surface hydroxylation as the annealing temperature increased. Similarly, the Ni 2p spectra showed a decrease in satellite peak intensity, indicating a transition to a more crystalline NiO structure. These results highlight the critical role of annealing temperature and Co doping in tailoring the structural and surface properties of NiO thin films, paving the way for their potential applications in advanced optoelectronic and energy devices.

Keywords: Cobalt, NiO thin films, Annealing temperature, Surface morphology, Grain growth, FESEM analysis.

INTRODUCTION

Transition metal oxides (TMOs) such as CuO, FeO, MnO, TiO_2, CoO and NiO exhibit unique properties, including the electrical insulation, antiferromagnetism and wide bandgap semiconductor behaviour, primarily due to their cubic lattice structures and partially filled *d*-shells. These materials are characterized by their tunable electronic and magnetic properties, which can be influenced by factors such as stoichiometry, synthetic methods and post-synthesis treatments [1,2]. The pressure-induced Mott transition in these oxides reveals complex interactions between the electronic correlations and the magnetic states, highlighting their potential for applications in electronics and energy storage [3].

The advancements in hybrid functional methods have improved the accuracy of predicting their band gaps, essential for optimizing their use in various technological applications [4,5]. Among the various TMOs, nickel oxide (NiO) has emerged as a promising p-type TCO, exhibiting significant potential for multifunctional device applications [6]. NiO possesses a wide bandgap ranging from 3.6 eV to 4.0 eV, ensuring the minimal absorption in the visible region, making it highly suitable for the optoelectronic applications [7]. Optimizing NiO films through various deposition methods, such as electron beam evaporation and magnetron sputtering, has led to impressive power conversion efficiencies. For example, sputtered NiO films, when treated with $NaIO_4$, showed improved crystallinity and achieved a power conversion efficiency of 23.22% in single-junction solar cells. Remarkably, these films reached 30.48% in tandem configurations. Furthermore, incorporating amino acid-complexed NiO has been shown to reduce interfacial recombination, resulting in efficiencies of 20.27% even under ambient conditions [8-11]. Also, the co-doping strategies with non-metal ions have also enhanced device performance, achieving efficiencies up to 16.20% [12]. These developments highlight the crucial role of NiO in boosting the perovskite solar cells performance. Its unique properties also make it ideal for use in energy conversion, gas sensing and electrochromic devices [11].

NiO thin films are also used in organic light-emitting diodes (OLEDs) due to their well-aligned hole energy levels, which enhance device stability and efficiency [13,14]. When NiO is doped with cobalt, it significantly boosts electroluminescence performance, leading to a 24.5% increase in current density and an 84.9% enhancement in brightness compared to traditional ITO anodes. Moreover, the use of lithium-doped NiO films has demonstrated improved electrical properties, which are crucial for efficient hole transport in OLED applications [15]. As well, the development of ultra-smooth NiO-based anodes has led to a 30.6% increase in efficiency for flexible OLEDs, highlighting the importance of surface properties in optimizing device performance [16]. Despite its wide range of uses, optimizing NiO thin films for advanced applications still presents some hurdles. A key challenge is the inherent resistivity of NiO, which typically falls between 10^{-2} and 10^{-3} Ω cm. This can restrict its effectiveness as a transparent conducting electrode [17,18].

Doping has been a key area of research for improving the electrical and optical performance of NiO. Many studies indicate that even small amounts of cobalt doping (1, 3 and 5 atomic percent) can boost conductivity and narrow the band gap from 3.80 eV to 3.76 eV. The best electrical resistivity is observed at a 3 atomic % cobalt concentration [18]. Moreover, annealing temperatures ranging from 200 ºC to 600 ºC further affect these properties; higher temperatures improve crystallinity and reduce the band gap to as low as 2.89 eV [19]. The films maintain high optical transmittance (up to 90%) at lower annealing temperatures, while the morphology transitions from spherical nanoparticles to larger grains with increased temperature [20]. The effect of annealing temperature on the structural, optical and electrical properties of NiO thin films remains a critical area of investigation. Studies have shown that annealing enhances crystallinity, increases grain size and reduces defect density, leading to improved conductivity and transparency. For instance, NiO films annealed at 500 ºC exhibited a grain size of 15.6 nm and resistivity of 1.8×10^{-3} Ω cm, compared to 10.2 nm and 3.4×10^{-3} Ω cm for films annealed at 300 ºC [21]. The primary objective of this study is to explore the influence of Co doping concentrations and synthesis annealing temperatures on the structural, optical and surface properties of NiO thin films. This study systematically investigates the effects of varying Co doping levels (1%, 3%, 5% and 7%) and annealing temperatures (400 ºC, 500 ºC and 600 ºC) on NiO thin films. X-ray photoelectron spectroscopy (XPS) was employed to identify the chemical states of Ni, Co, O and to detect binding energy shifts associated with different doping concentrations and annealing conditions. The impact of Co incorporation on the NiO lattice was analyzed to understand the changes in crystallinity and structural properties. Moreover, UV-Visible spectroscopy was also used to optimize the optical properties by identifying the ideal combination of doping level and annealing temperature for band gap tuning.

EXPERIMENTAL

The nickel acetate tetrahydrate [$Ni(CH_3COO)_2 \cdot 4H_2O$] was used as the precursor for synthesizing NiO thin films. Ethanol was selected as the solvent due to its low volatility and ability to form a homogenous precursor solution. Citric acid ($C_6H_8O_7$) was utilized as a stabilizer to prevent premature precipitation during the synthesis process and ensure uniformity. Glass substrates with dimensions of 25.4 mm × 76.2 mm were cleaned thoroughly to achieve high adhesion of the films. For doped films, cobalt(II) nitrate hexahydrate [$Co(NO_3)_2 \cdot 6H_2O$] was employed as doping agent to study the effect of doping on film properties.

Synthesis of NiO thin films with sol-gel spin coating process: The fabrication of Co-doped NiO thin films was carried out using the sol-gel method combined with spin-coating, a widely employed technique for producing high-quality thin films [22]. Initially, nickel nitrate hexahydrate was used as precursor for NiO, while cobalt nitrate hexahydrate served as source for Co doping. Both precursors were dissolved in a mixture of deionized water and ethanol to ensure homogeneity, followed by the addition of citric acid as a complexing agent. The resulting solution was stirred continuously at room temperature to achieve a clear and stable sol. To prepare the Co-doped NiO films, the desired concentration of cobalt (1%, 3%, 5% and 7% molar ratio) was introduced into the solvent and the mixture was stirred for an additional 2 h. The prepared sol was then aged to improve its viscosity and stability, ensuring uniform film deposition.

The spin-coating process was employed to deposit the sol onto cleaned glass substrates. Prior to deposition, the substrates were thoroughly cleaned using a sequential process involving acetone, ethanol and deionized water to remove impurities and enhance adhesion. During spin coating, the sol was dispensed onto the substrate, which was then rotated at a speed of 3000 rpm for 30 sec to spread the solution uniformly. This step was repeated to achieve the desired film thickness. After deposition, the coated substrates were dried at 100 ºC for 10 min to remove residual solvents. The dried films were then annealed at varying temperatures (400 ºC, 500 ºC and 600 ºC) in a muffle furnace for 2 h to improve crystallinity and eliminate organic residues. A programmable temperature controller was used to maintain a consistent heating rate and stabilize the temperature during the process. After annealing, the samples were allowed to cool gradually to room temperature within the furnace to minimize the thermal stresses and potential microstructural distortions. This setup ensured repeatability and uniform treatment across all samples. This combined sol-gel and spin-coating approach provided a cost-effective and efficient method for fabricating Co-doped NiO thin films with controlled composition and surface morphology. The spin coating and annealing parameters are given in Table-1.

TABLE-1
SPIN COATING AND ANNEALING PARAMETERS

Parameter	Value
Precursor concentration	0.2 M
Spin speed	3000 rpm
Spin duration	40 sec
Annealing temperature	400, 500, 600 ºC
Annealing duration	2 h
Film thickness	~ 300 nm

Characterization techniques

Texture coefficient: The XRD Bruker D8 instrument with Cu*K*α X-ray source was used for the sample analysis. The texture coefficient is computed to illustrate the favoured alignment of the films through the subsequent formula [18]:

$$TC_{hkl} = \frac{I_{(hkl)}/I_{0(hkl)}}{\left(\frac{1}{N}\right)\sum_N I_{(hkl)}/I_{0(hkl)}}$$

where TC_{hkl} = texture coefficient for *hkl* plane; I_{hkl} = intensity of the *hkl* plane in sample; $I_{0(hkl)}$ = intensity of the *hkl* plane in bulk or standard reference (*e.g.*, JCPDS card); N = number of diffraction peaks considered.

Optical analysis: Once the thin films were prepared, they were placed in the path of the light beam in a UV-Visible spectrophotometer (Shimadzu UV-1800), which measured the absorption or transmission of light as it passed through the samples, with measurements recorded as a function of wavelength. The resulting data were used to evaluate the optical properties of the films, including their optical transmittance and band gap energy. Using Tauc's method, the band gap was determined to be approximately 1.5 eV, aligning well with the solar spectrum.

$$(\alpha h\nu)^2 = A(h\nu - E_g)$$

where α is the absorption coefficient, hν is the photon energy, A is a constant and E_g is the bandgap energy.

XPS analysis: The XPS spectrum was measured using an ESA-31 spectrometer with a 180º hemispherical electrostatic analyzer (250 mm radius), capable of 10-500 eV pass energy and 1.5 eV resolution at 5 keV. The setup included a multi-element zooming lens and normal sample alignment for precise surface measurements. Tungsten films were sputter-deposited on SiO_2 substrates using 2 keV argon ions at a base pressure of 1×10^{-7} mbar, with *in situ* thickness monitoring *via* quartz crystal.

RESULTS AND DISCUSSION

Texture coefficient: The variations of TC_{hkl} for NiO and Co-doped NiO (1%, 3%, 5% and 7%) thin films for different annealing temperature and the recorded intensity I_{hkl} for the planes (111), (200), (220), (311) and (222) from XRD patterns for Co-doped NiO (1%, 3%, 5% and 7%) at each annealing temperature (400 ºC, 500 ºC, 600 ºC) are presented in Table-2. The texture coefficient TC_{hkl} provides insight into the crystallographic orientation of thin films. A TC_{hkl} value equal to 1 indicates a random orientation, where no specific crystallographic plane dominates the texture of film. When $TC_{hkl} > 1$, it signifies a preferred orientation along the corresponding *hkl* plane, meaning that this plane is more prominently aligned compared to a randomly oriented sample. Conversely, a $TC_{hkl} < 1$indicates a suppressed orientation along the *hkl* plane, suggesting that this plane is less favourably aligned within the film structure. It is essential to highlight that the doping procedure influenced the preferred alignment. It was observed that while the undoped NiO films display two dominant growth orientations along the (111) and (222) planes, the Co-doped film predominantly exhibits a single preferred growth direction along the (111) plane. The reorientation effect of crystals in a given *hkl* direction due to doping processes is a complex phenomenon influenced by various factors, as evidenced by multiple studies [23].

The texture coefficients (TC) of NiO films annealed at 400 ºC, 500 ºC and 600 ºC across crystallographic planes: (111), (200), (220), (311) and (222) are analyzed. As shown in Fig. 1a, the TC (111) values for pure NiO films consistently increased with temperature, reaching 2.65, 2.7 and 2.75 at 400 ºC, 500 ºC and 600 ºC, respectively. This indicates a strong preference for crystal growth along the (111) plane. Conversely, the TC values for the other planes were much lower, suggesting suppressed crystal orientations in those directions. Specifically, TC (200) ranged from 0.22 to 0.27, TC (220) from 0.24 to 0.35, TC (311) from 0.26 to 0.32 and TC (222) from 1.35 to 1.44. Fig. 1b illustrates the TC (111) values for Co-doped NiO films at varying doping levels (1%, 3%, 5% and 7%) and annealing temperatures. At 400 ºC, the TC (111) values were 2.68, 2.72, 2.74 and 2.79 for 1%, 3%, 5% and 7% doping levels, respectively. At 500 ºC, these values increased to 2.71, 2.75, 2.78 and 2.82, while at 600 ºC, they remained high, ranging from 2.72 to 2.84. These results confirm

TABLE-2
TEXTURE COEFFICIENTS TC_{hkl}, OF Co-DOPED NiO THIN FILMS FOR DIFFERENT ANNEALING TEMPERATURES

Sample	Annealing temp. (ºC)	Plane (111)	Plane (200)	Plane (220)	Plane (311)	Plane (222)
Pure NiO	400	2.65	0.27	0.35	0.29	1.44
	500	2.70	0.25	0.32	0.26	1.40
	600	2.75	0.22	0.30	0.24	1.35
1% Co-NiO	400	2.68	0.26	0.34	0.28	1.42
	500	2.73	0.24	0.31	0.25	1.38
	600	2.78	0.21	0.28	0.22	1.33
3% Co-NiO	400	2.70	0.25	0.33	0.27	1.40
	500	2.75	0.23	0.30	0.24	1.36
	600	2.80	0.20	0.27	0.21	1.30
5% Co-NiO	400	2.72	0.24	0.32	0.26	1.38
	500	2.77	0.22	0.29	0.23	1.34
	600	2.82	0.19	0.26	0.20	1.28
7% Co-NiO	400	2.74	0.23	0.31	0.25	1.36
	500	2.79	0.21	0.28	0.22	1.32
	600	2.84	0.18	0.25	0.19	1.26

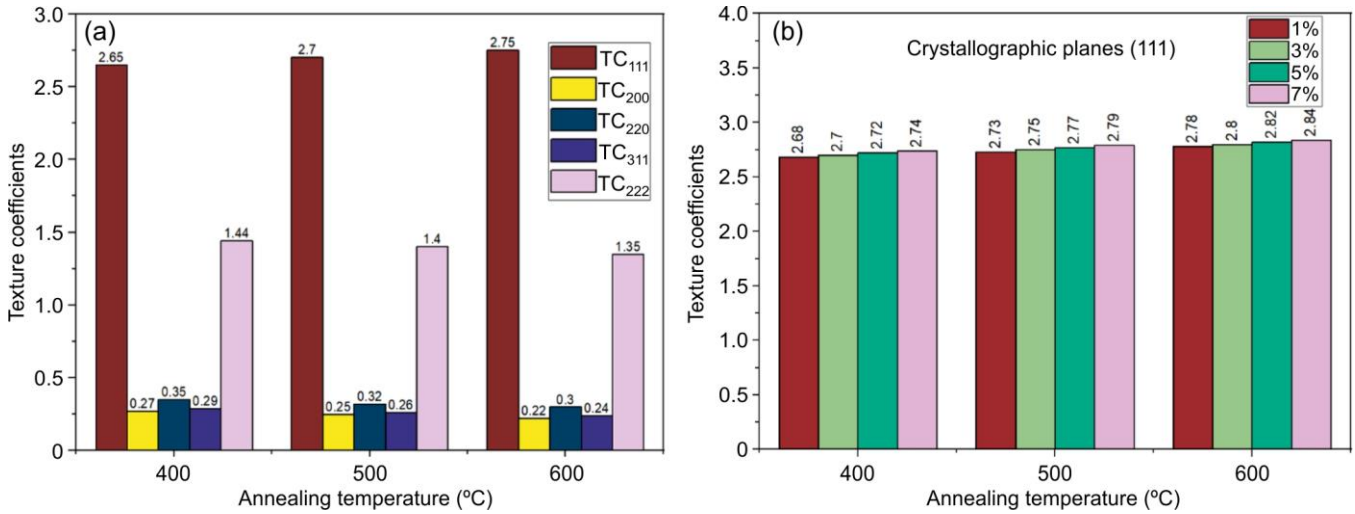

Fig. 1. Texture coefficients (a) Pure NiO (b) Co doped NiO

that both annealing temperature and Co doping enhance the preferred orientation along the (111) plane, with the highest TC (111) observed at higher doping levels and temperatures. This indicates the significant role of doping and thermal treatment in tailoring the texture of NiO films [22].

Optical properties

UV-visible spectroscopy: Fig. 2a-b shows the UV-Visible spectroscopy analysis of transmission and absorbance spectra of pure NiO thin film for various annealing temperature. As resulting, the transmittance percentage increases trend was observed due to increasing annealing temperature (400 ºC to 600 ºC). This can be attributed to the growth in crystallite size linked to the enhanced densification of the film [24-26] and might result from reduced defect scattering. The thickness of the thin film is influenced by the annealing temperature. In this study, the newly deposited NiO thin film exhibits amorphous properties. During the annealing process, unsaturated defects and localized states are progressively eliminated, facilitating the development of numerous structural bonds. The reduction in unsaturated defects consequently decreases the density of localized states. This improvement in crystallinity and structural arrangement leads to a reduction in the thickness of film [27,28].

As the annealing temperature increases, the thickness of the NiO thin films reduces [29,30]. Throughout the annealing process, the thin film undergoes a transition to a more organized phase, leading to a reduction in defects. This transformation induces shrinkage, which ultimately results in a decrease in the thickness of film.

The Tauc plot of $(\alpha h\nu)^2$ with respect to the photon energy ($h\nu$) were used to obtained the band gap energy for pure NiO shown in Fig. 3. It is clearly showed that decreases in band gap energy due to increasing annealing temperature 400 ºC to 600 ºC. The narrowing of the energy band gap at increased annealing temperatures could be linked to the expansion of crystallite dimensions and the reduction of defect locations. With the elevation of the annealing temperature, the crystalline dimensions of the NiO thin films are observed to expand within the spectrum of 11.5-15.68 nm, leading to a reduction

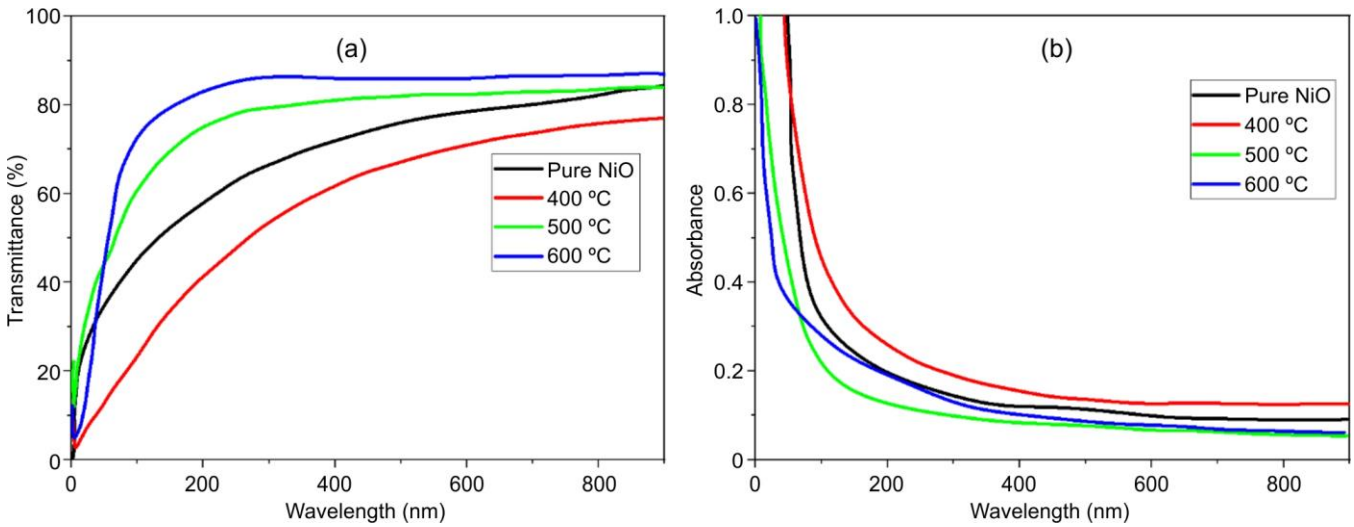

Fig. 2. UV-Visible transmittance spectra of pure NiO thin films. The plot will show the impact of annealing and the determination of the bandgap

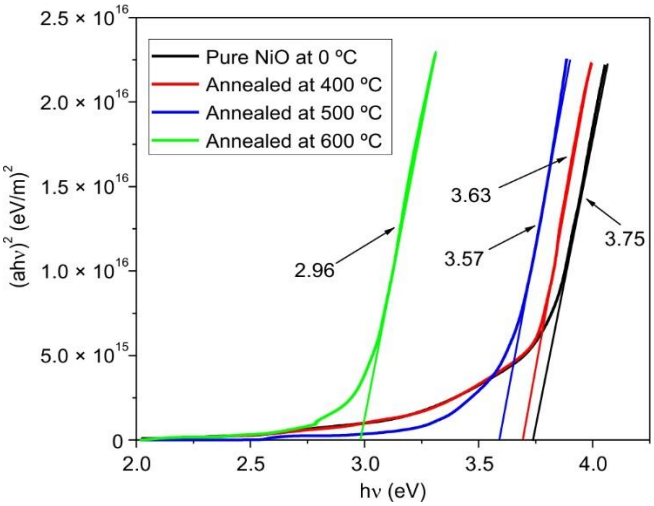

Fig. 3. Tauc plot of $(\alpha h\nu)^2$ *versus* photon energy (hν) for pure NiO thin film

in the band gap energy of the specimens, attributed to the phenomenon of quantum confinement.

The quantum confinement effect occurs when the size of a material's crystallites becomes comparable to or smaller than the exciton Bohr radius. In such small dimensions, the motion of electrons and holes is restricted, causing discrete energy levels to form instead of a continuous energy band. This confinement increases the energy difference between the valence and conduction bands, effectively widening the band gap. As the crystallite size decreases, the band gap energy increases due to this phenomenon. The computed value of the band gap energy presented in Table-3 aligns closely with the band gap of bulk NiO (3-4 eV). A typical phenomenon seen in annealed direct-transition semiconductor thin films is the reduction in optical band gap energy [31]. The reduction in band gap with increasing annealing temperature can be attributed to the improvement in crystalline quality (growth of larger crystallites), as confirmed by the results of XRD analyses.

TABLE-3
BAND GAP FOR NiO AND Co-DOPED NiO FOR VARIOUS ANNEALING TEMPERATURE (400, 500 AND 600 ºC)

Thin film	Band gap (eV)		
	400 ºC	500 ºC	600 ºC
Pure NiO	3.75	3.7	2.96
1% Co-doped NiO	3.7	3.65	3.6
3% Co-doped NiO	3.65	3.6	3.55
5% Co-doped NiO	3.6	3.55	3.5
7% Co-doped NiO	3.55	3.5	3.45

Fig. 4 presents the UV-visible spectroscopic analysis of the transmission spectra and absorbance of Co-doped NiO thin films at different annealing temperatures. The UV-visible spectrophotometric analysis demonstrates the influence of annealing temperature and Co doping on the optical properties of NiO thin films. The transmission spectra reveal that pure NiO exhibits lower transmittance compared to Co-doped films, with transmittance increasing progressively with higher doping concentrations. At 400 ºC, the films show the moderate transmittance, which significantly improves at 500 ºC, with 7% Co-doped NiO displaying the highest transmittance due to enhanced crystallinity and reduced defect states. At 600 ºC, the transmittance peaks for most samples, though a slight decline is observed for higher doping levels, likely due to agglomeration or structural distortions. The absorbance spectra further confirm these trends, indicating improved optical activity with increased doping and annealing temperature, which enhances the structural and optical quality of the thin films. Generally, particle size tends to show an inverse correlation with band gap energy. During the annealing process, as the annealing temperature increases, a noticeable reduction in band gap energy occurs. This behaviour suggests a steady decrease in band gap energy, which can be attributed to the intriguing influence of the surface plasmon resonance (SPR) effect. Furthermore, the absorption edge shifted smoothly toward the shorter wavelength region. This observation suggests the impact of quantum confinement, resulting in a widening of the band gap in NiO upon the incorporation of cobalt metal ions.

Fig. 5 shows the Tauc plot of $(\alpha h\nu)^2$ energy band gap with respect to photon energy (hν) at different concentrations (1%, 3%, 5% and 7%) for different annealing temperature 400 ºC ºC, 500 ºC and 600 ºC, respectively. The Tauc plots for Co-doped NiO thin films annealed at 400 ºC, 500 ºC and 600 ºC demonstrate a clear shift in the optical band gap with increasing annealing temperature and Co doping concentration. At 400 ºC, the band gap values range from 3.70 eV for pure NiO to 3.55 eV for 7% Co-doped NiO, indicating a reduction in the band gap with higher Co doping. A similar trend is observed at 500 ºC, where the band gap decreases from 3.65 eV to 3.50 eV and at 600 ºC, where the band gap narrows further from 3.60 eV to 3.45 eV with increased doping [22].

This reduction in the band gap can be attributed to the substitution of Ni^{2+} ions with Co^{2+} ions, which introduces the localized energy levels within the band gap. Moreover, the annealing process enhances the crystallinity and reduces defect density, further influencing the optical properties. The observed shift in the band gap with increasing Co doping concentration and annealing temperature suggests a modulation of the electronic structure, likely due to the incorporation of cobalt ions and improved film quality. These findings are consistent with the quantum confinement effect and the surface plasmon resonance phenomenon, which are known to influence the optical band gap in doped thin films. Overall, the results indicate that Co doping and annealing temperature play a significant role in tuning the optical properties of NiO thin films, making them suitable for applications in the optoelectronic devices.

Surface properties: Fig. 6a-f shows the XPS analysis of NiO for different annealing temperature as prepared by sol-gel process with spin-coating method. The XPS spectrum shows the presence of O 1s and Ni (2p), which consists of two variants ($2p_{3/2}$ and $2p_{1/2}$) due to spin orbit splitting. The binding energy of Ni (2p) peaks as seen in Fig. 6d-f at 856.53 eV and 867.32 eV for Ni $(2p)_{3/2}$ and Ni $(2p)_{1/2}$, respectively. As the annealing temperature increases, the satellite peaks diminish and the NiO peaks become sharper, signifying the dominance of Ni^{2+} in a well-ordered NiO lattice. The peak deconvolution highlights a consistent trend of reduced satellite intensity with increasing annealing temperature, further confirming enhanced crystallinity and reduced defects.

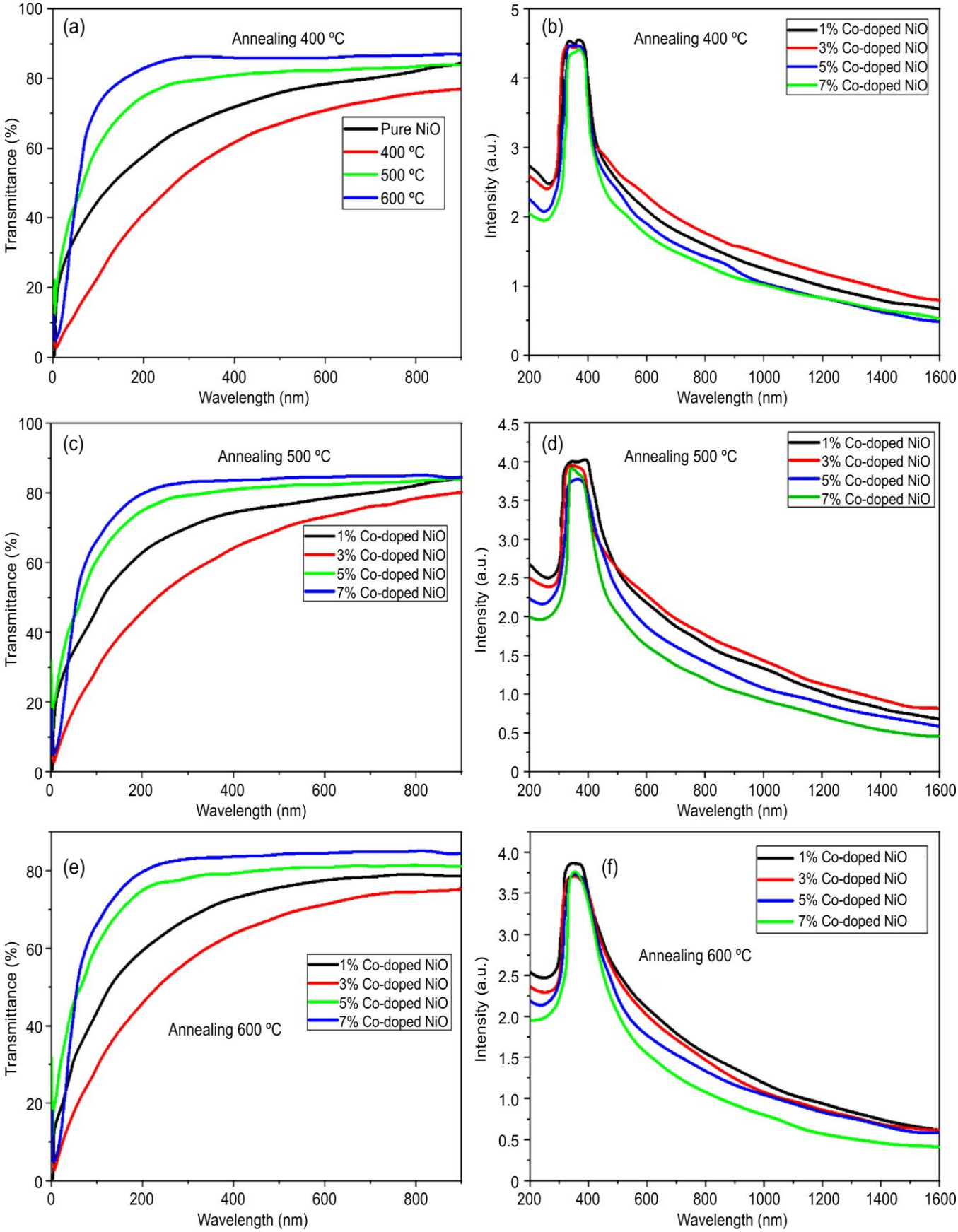

Fig. 4. UV-Visible transmittance spectra of Co-doped NiO (1%, 3%, 5% and 7%) thin films. The plot will show the impact of annealing temperature (400, 500 and 600 ºC) and the determination of the bandgap

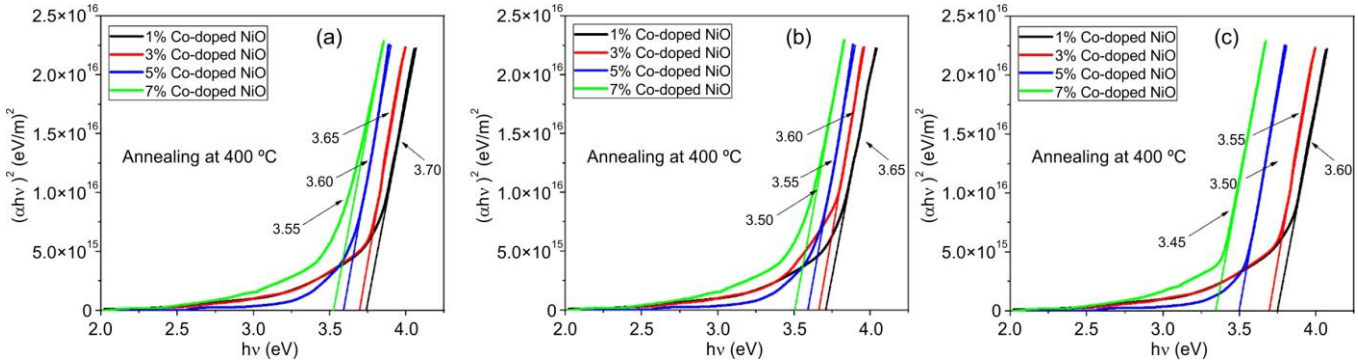

Fig. 5. Tauc plot of $(\alpha h\nu)^2$ *versus* photon energy (hν) for Co-doped NiO thin film

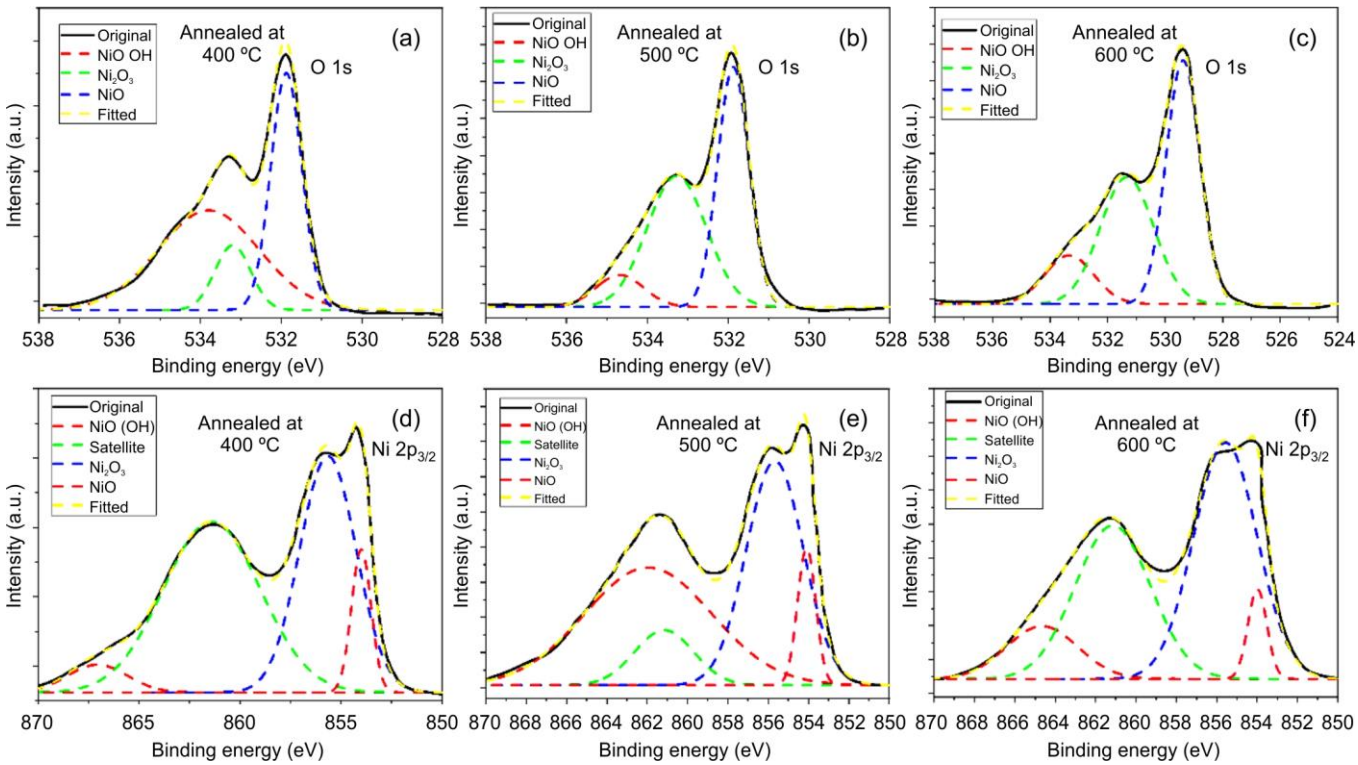

Fig. 6. XPS (a-c) spectrum O 1s at 400, 500 and 600 ºC, (d-f) Ni 2p at different annealing temperature 400, 500 and 600 ºC

The presence of the Ni^{2+} cation leads to an increase in these peaks, resulting from the charge transfer from oxygen to nickel. Moreover, a satellite shake-up peak is identified at 865.3 eV, attributed to the simultaneous emission of a photon-electron and the excitation of a valence electron to a higher vacant bound state. It can be reflecting the oxidation state Ni change to 2+ in NiO thin film. The peak centered at approximately 530 eV is attributed to lattice oxygen (NiO), whereas the peaks around 531.5 eV and 533 eV are associated with Ni_2O_3 and surface hydroxyl groups (NiO(OH)), respectively. Meanwhile, the peak at 532 eV highlights the presence of surface impurities, including carbon-based oxides and hydroxyl groups (H-O-H) formed from residual water molecules [32,33]. A gradual shift in the relative intensities of these peaks is observed with increasing annealing temperature. At 600 ºC, the spectra show significant contributions from hydroxyl groups, indicating incomplete oxidation of the Ni precursor. As the annealing temperature increases to 500 ºC and 600 ºC, the intensity of the lattice oxygen peak becomes dominant, suggesting improved crystallinity and reduced surface hydroxylation. The presence of Ni_2O_3 is consistent across all samples, indicating the partial oxidation of NiO [22].

Fig. 7a-d presents the full XPS spectrum of Co-doped NiO thin films with different concentrations (1%, 3%, 5% and 7%), revealing the presence of Ni, Co, O and C. Detailed analysis of the XPS survey for various elements for annealing temperature is illustrated in Fig. 7, which includes specific wide spectra for C 1s, O 1s, Ni 2p and Co 2p, respectively.

Fig. 7a shows the C 1s spectra for all Co-doped NiO thin films. The carbon signal is primarily attributed to residual carbon from the sample preparation and incidental hydrocarbon contamination from the XPS instrument. Peaks are observed at binding energies of ~284.46 eV (C–C/C–H bonds), ~285.02 eV (C–O bonds) and ~289.24 eV (O–C=O bonds). The consistency of these peaks across all samples indicates negligible influence of Co doping concentration on

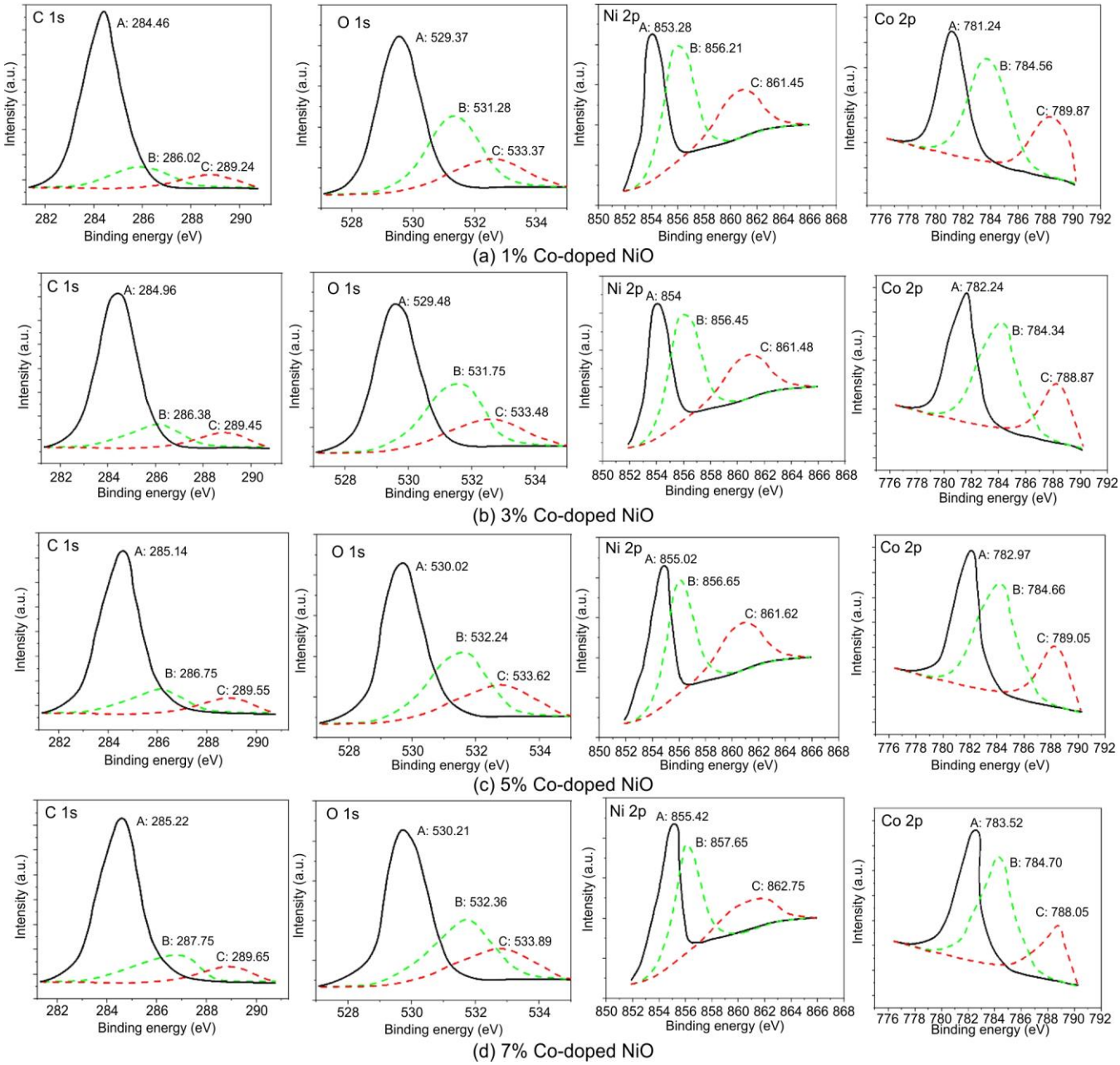

Fig. 7. XPS spectra of C 1s, O 1s, Ni 2p and Co 2p for the Co-doped NiO (1%, 3% 5% and 7%)

carbon contamination. Fig. 7a depicts the carbon spectra of 1% Co: NiO, attributed to residual carbon from the sample as well as unintended hydrocarbons originating from the XPS analysis. Fig. 7b shows the O1s spectrum of 1% Co-doped NiO films, featuring two main peaks: peak A at 529.37 eV, associated with NiO and peak B at 531.28 eV, linked to Ni–OH bonds. Similarly, for 3% Co: 529.48 eV (Ni–O), 531.75 eV (Ni–OH), 5% Co: 530.02 eV (Ni–O), 532.24 eV (Ni–OH), 7% Co: 530.21 eV (Ni–O), 532.36 eV (Ni–OH), respectively. The increase in binding energy with higher Co concentrations indicates enhanced interaction between Co and oxygen atoms in the NiO lattice. The Ni 2p spectra (Fig. 7c) exhibit three distinct peaks corresponding to Ni^{2+}, Ni^{3+} and satellite structures. The binding energies for 1% Co: 854.05 eV (Ni^{2+}), 855.92 eV (Ni^{3+}), 860.70 eV (satellite), 3% Co: 854.08 eV (Ni^{2+}), 855.95 eV (Ni^{3+}), 860.72 eV (satellite), 5% Co: 854.10 eV (Ni^{2+}), 855.98 eV (Ni^{3+}), 860.74 eV (satellite), 7% Co: 854.12 eV (Ni^{2+}), 856.00 eV (Ni^{3+}), 860.76 eV (satellite), respectively [22]. The presence of Ni^{2+} and Ni^{3+} states confirms the coexistence of multiple oxidation states, which contributes to the electrical and optical properties of the films. The satellite peaks further support the high crystallinity of the NiO matrix. The Co 2p spectra (Fig. 7d) reveal characteristic peaks for CoO. The binding energies for Co $2p_{3/2}$ and Co $2p_{1/2}$ peaks are as follows: 1% Co: 780.50 eV (Co $2p_{3/2}$), 796.98 eV (Co 2p1/2), 3% Co: 780.51 eV (Co $2p_{3/2}$), 797.00 eV (Co $2p_{1/2}$), 5% Co: 780.52 eV (Co $2p_{3/2}$), 797.02 eV (Co $2p_{1/2}$), 7% Co: 780.55 eV (Co $2p_{3/2}$), 797.05 eV (Co $2p_{1/2}$). The Co 2p peaks confirm the successful incorporation of cobalt into the NiO lattice, with slight shifts in

binding energy indicating increasing interaction strength with higher Co concentrations [22,34].

The O 1s spectra for all annealing conditions exhibit multiple peaks corresponding to different oxygen species. The peak centered at approximately 530.0 eV is attributed to lattice oxygen (NiO), whereas the peaks around 531.5 eV and 533.0 eV are associated with Ni_2O_3 and surface hydroxyl groups (NiO(OH)), respectively. A gradual shift in the relative intensities of these peaks is observed wisth increasing annealing temperature. At 400 ºC, the spectra show significant contributions from hydroxyl groups, indicating incomplete oxidation of the Ni precursor. As the annealing temperature increases to 500 ºC and 600 ºC, the intensity of the lattice oxygen peak becomes dominant, suggesting improved crystallinity and reduced surface hydroxylation. The presence of Ni_2O_3 is consistent across all samples, indicating the partial oxidation of NiO. The observed increase in grain size with higher annealing temperatures indicates an improvement in the crystal quality of the thin films. These results demonstrate that annealing temperature plays a crucial role in influencing the surface morphology and crystallinity of NiO thin films [35].

Conclusion

This study elucidates the effective utilization of citric acid based chelating approach to study the impact of Co doping concentration and annealing temperature on the structural, chemical and surface properties of NiO thin films. The texture coefficients TC_{hkl} for NiO thin films showed a significant dependence on annealing temperature, reflecting changes in crystallographic orientation and film structure. The (111) plane exhibited the highest TC_{hkl}, confirming the preferential *c*-axis orientation of the NiO thin films, particularly at 500 ºC. The annealing temperature of 500 ºC was found to be optimal for achieving superior crystallinity and texture, with the highest TC_{hkl} values for the (111) plane. XPS analysis confirmed the successful incorporation of cobalt into the NiO lattice, with Co and Ni existing in stable oxidation states. The binding energy shifts observed in Ni 2p, O 1s and Co 2p spectra underscore the strong interaction between Co dopants and the NiO matrix. These experimental results underscore the significance of controlled doping and annealing in optimizing the propwww in energy storage, sensors and electronic devices.

CONFLICT OF INTEREST

The authors declare that there is no conflict of interests regarding the publication of this article.

REFERENCES

1. S.O. Ogungbesan, N.O. Etafo, O.H. Anselm, M. Kalulu, M. Abdullah, O. Ejeromedoghene, D.D. Diaz and G. Fu, *J. Mol. Struct.*, **1337**, 142209 (2025); https://doi.org/10.1016/j.molstruc.2025.142209
2. R.R. Poolakkandy and M.M. Menamparambath, *Nanoscale Adv.*, **2**, 5015 (2020); https://doi.org/10.1039/d0na00599a
3. I. Leonov, A.O. Shorikov, V.I. Anisimov and I.A. Abrikosov, *Phys. Rev. B*, **101**, 245144 (2020); https://doi.org/10.1103/PhysRevB.101.245144
4. P. Liu, C. Franchini, M. Marsman, and G. Kresse, *J. Phys.: Condens. Matter*, **32**, 015502 (2020); https://doi.org/10.1088/1361-648X/ab4150
5. L. Chen, Z. Liu, Z. Guo and X.-J. Huang, *J. Mater. Chem. A Mater. Energy Sustain.*, **8**, 17326 (2020); https://doi.org/10.1039/D0TA05539E
6. Karishma, N. Tripathi, R.K. Pandey, A. Tripathi, K. Asokan, V. Bhushan and V. Sharma, *Energy Storage*, **6**, 70065 (2024); https://doi.org/10.1002/est2.70065
7. M.I. Hossain and B. Aissa, *Processess*, **12**, 2809 (2024); https://doi.org/10.20944/preprints202411.1284.v1
8. K.O. Egbo, C.E. Ekuma, C.P. Liu and K.M. Yu, *Phys. Rev. Mater.*, **4**, 104603 (2020); https://doi.org/10.1103/PhysRevMaterials.4.104603
9. M. Napari, T.N. Huq, T. Maity, D. Gomersall, K.M. Niang, A. Barthel, J.E. Thompson, S. Kinnunen, K. Arstila, T. Sajavaara, R.L.Z. Hoye, A.J. Flewitt and J.L. MacManus-Driscoll, *InfoMat*, **2**, 769 (2020); https://doi.org/10.1002/inf2.12076
10. Y. Jin, H. Feng, Y. Li, H. Zhang, X. Chen, Y. Zhong, Q. Zeng, J. Huang, Y. Weng, J. Yang, C. Tian, J. Zhang, L. Xie and Z. Wei, *Adv. Energy Mater.*, **15**, 2403911 (2025); https://doi.org/10.1002/aenm.202403911
11. D.S. Mann, S. Thakur, S.S. Sangale, K.-U. Jeong, S.-N. Kwon and S.-I. Na, *Small*, **20**, 2405953 (2024); https://doi.org/10.1002/smll.202405953
12. J. Dong, S. Guo, Z. He, Z. Jiang and J. Jia, *J. Solid State Chem.*, **339**, 124948 (2024); https://doi.org/10.1016/j.jssc.2024.124948
13. J. Kim, H.J. Park, C.P. Grigoropoulos, D. Lee and J. Jang, *Nanoscale*, **8**, 17608 (2016); https://doi.org/10.1039/c6nr04643f
14. W.-S. Chen, S.-H. Yang, W.-C. Tseng, W. W.-S. Chen, and Y.-C. Lu, *ACS Omega*, **6**, 13447 (2021); https://doi.org/10.1021/acsomega.1c01618
15. S.-H. Yang, H.-Y. Lin, C.-C. Ho and J.-H. Guo, *Opt. Mater.*, **154**, 115773 (2024); https://doi.org/10.1016/j.optmat.2024.115773
16. V.H. López-Lugo, M. García-Hipólito, A. Rodríguez-Gómez and J.C. Alonso-Huitrón, *Nanomaterials*, **13**, 197 (2023); https://doi.org/10.3390/nano13010197
17. Y. Bai, Y. Chuai, Y. Wang and Y. Wang, *Micromachines*, **13**, 1511 (2022); https://doi.org/10.3390/mi13091511
18. M. Touati, T. Boucherka, A. Barbadj, N. Brihi and F. Labreche, *Opt. Mater.*, **143**, 114235 (2023); https://doi.org/10.1016/j.optmat.2023.114235
19. N.R. Aswathy, J. Varghese and R. Vinodkumar, *J. Mater. Sci.: Mater. Electron.*, **31**, 16634 (2020); https://doi.org/10.1007/s10854-020-04218-5
20. wT. Ivanova, A. Harizanova, M. Shipochka and P. Vitanov, *Materials*, **15**, 1742 (2022); https://doi.org/10.3390/ma15051742
21. M.Y. Khan, M.W. Akhtar, M.F.A. Khan, Z. Abbass, F. Rasheed, M.S. Ali, N. Pirzada and R. Shahbaz, *Mehran Univ. Res. J. Eng. Technol.*, **43**, 150 (2024); https://doi.org/10.22581/muet1982.3149
22. V.R. Jayalakshmi, M.P. Pachamuthu and N. Jeyakumaran, *Malays. J. Chem.*, **27**, 306 (2025); https://doi.org/10.55373/mjchem.v27i3.306
23. X. Luo, R. Li, X. Ma, Y. Chen, B. Kang, J. Zhang, W. Ren, Z. Feng and S. Cao, *J. Phys. Condens. Matter*, **33**, 275803 (2021); https://doi.org/10.1088/1361-648X/abfd53
24. T.M. Tsai, C.C. Lin, W.C. Chen, C.H. Wu, C.C. Yang, Y.F. Tan, P.Y. Wu, H.C. Huang, Y.C. Zhang, L.C. Sun and S.Y. Chou, *J. Alloys Compd.*, **826**, 154126 (2020); https://doi.org/10.1016/j.jallcom.2020.154126
25. N.R. Aswathy, J. Varghese and R. Vinodkumar, *J. Mater. Sci. Mater. Electron.*, **31**, 16634 (2020); https://doi.org/10.1007/s10854-020-04218-5
26. M.M. Gomaa, G. Reza-Yazdi, M. Rodner, G. Greczynski, M. Boshta, M.B.S. Osman, V. Khranovskyy, J. Eriksson and R. Yakimova, *J. Mater. Sci. Mater. Electron.*, **29**, 11870 (2018); https://doi.org/10.1007/s10854-018-9287-6

27. F. Hajakbari, M. Taheri Afzali and A. Hojabri, *Acta Phys. Pol. A*, **131**, 417 (2017); https://doi.org/10.12693/APhysPolA.131.417
28. C.H. Hsu, K.T. Chen, P.H. Huang, W.Y. Wu, X.Y. Zhang, C. Wang, L.S. Liang, P. Gao, Y. Qiu, S.Y. Lien, Z.B. Su, Z.-R. Chen and W.-Z. Zhu, *Nanomaterials*, **10**, 1322 (2020); https://doi.org/10.3390/nano10071322
29. M.A. Chougule, S.G. Pawar, P.R. Godse, R.D. Sakhare, S. Sen and V.B. Patil, *J. Mater. Sci. Mater. Electron.*, **32**, 24584 (2021); https://doi.org/10.1007/s10854-021-06919-x
30. S. Yang, Y. Liu, Y. Zhang and D. Mo, *Bull. Mater. Sci.*, **33**, 209 (2010); https://doi.org/10.1007/s12034-010-0032-x
31. V.P. Patil, S. Pawar, M. Chougule, P. Godse, R. Sakhare, S. Sen and P. Joshi, *J. Surf. Eng. Mater. Adv. Technol.*, **1**, 35 (2011); https://doi.org/10.4236/jsemat.2011.12006
32. J. Feldl, M. Budde, C. Tschammer, O. Bierwagen and M. Ramsteiner, *J. Appl. Phys.*, **127**, 235105 (2020); https://doi.org/10.1063/5.0006085
33. L. Cao, D. Wang and R. Wang, *Mater. Lett.*, **132**, 357 (2014); https://doi.org/10.1016/j.matlet.2014.06.114
34. M.A.R. Abdullah, M.H. Mamat, A.S. Ismail, M.F. Malek, S.A.H. Alrokayan, H.A. Khan and M. Rusop, *AIP Conf. Proc.*, **1733**, 020013 (2016); https://doi.org/10.1063/1.4948831
35. A.D. Raj, T. Pazhanivel, P.S. Kumar, D. Mangalaraj, D. Nataraj and N. Ponpandian, *Curr. Appl. Phys.*, **10**, 531 (2010); https://doi.org/10.1016/j.cap.2009.07.015